Proceedings of Global Power and Propulsion Society
ISSN-Nr: 2504-4400
GPPS Hong Kong 2023
October 17-19, 2023
www.gpps.global

# GPPS-TC-2023-0112

# NUMERICAL STABILITY ANALYSIS OF SOLUTION METHODS FOR STEADY AND HARMONIC BALANCE EQUATIONS

**Yuxuan Zhang**
**Northwestern Polytechnical University**
yuxuanzhang@mail.nwpu.edu.cn
Xi'an, Shaanxi, China

**Dingxi Wang**
**Northwestern Polytechnical University**
dingxi_wang@nwpu.edu.cn
Xi'an, Shaanxi, China

## ABSTRACT

This study presents an investigation into the stability and convergence properties of solution methods for the steady and unsteady Euler equations. A central scheme with artificial dissipation is used for the spatial discretization, and a Runge-Kutta scheme with or without implicit residual smoothing, such as LU-SGS for a steady solution and LU-SGS/BJ for an unsteady solution, is used for time integration. Both the von Neumann and matrix methods are used to analyze the stability of the involved solution methods. The stability of these schemes obtained by the two stability analysis methods is identical for periodic boundary conditions as expected. However, with inlet, outlet and slip wall boundary conditions, the stability can be analyzed using the matrix method only. It is found that these boundary conditions enhance stability of solution methods. Additionally, the matrix method can also allow for the analysis of the impacts of non-uniformity in grids and flow fields, as well as second-order artificial dissipation. For the unsteady Euler equations solved using the harmonic balance method, the stability analysis demonstrates that the time spectral source term must be handled implicitly to avoid instability for analysis with high grid-reduced frequency. The conclusions can be readily extended to the RANS equations and verified in a nozzle and the NASA rotor 37.

## INTRODUCTION

Nowadays, design of turbomachinery highly relies on computational fluid dynamics(CFD) for analyzing its performance by solving the steady and unsteady Euler equations or Reynolds-averaged Navier-Stokes(RANS) equations. In a numerical analysis, the robustness and convergence rate of involved solution methods are vitally important for design engineers, as they largely dictate the accomplishment of a design task. Typically, there are two kinds of numerical methods for pseudo-time integration: explicit methods and implicit methods. The representative explicit methods are the multi-stage Runge-Kutta methods (Jameson et al., 1981). Their advantages lie in the low memory consumption, low CPU cost per iteration and easy implementation. Because of this, it has been very popular in the CFD community. The biggest disadvantage of the explicit methods is its conditional stability. To achieve a stable solution, the time step is limited by the Courant-Fredrichs-Levy(CFL) stability condition. This time step limit is manifested by flow fields at off-design conditions and harmonic balance analysis with big grid-reduced frequency(Hall et al., 2013).

The implicit methods, on the other hand, often have high memory consumption, high CPU cost per iteration and are much more difficult to be implemented, when compared with the explicit methods. The biggest advantage of the implicit methods is better stability. Thus a much bigger time step can be allowed in an analysis leading to reduced overall time cost. The extended stability depends on the approximation of the system Jacobian matrix. A better approximation generally leads to higher stability but incurs more implementation complexity and computing resources.

The Lower Upper Symmetric Gauss Seidel(LU-SGS) method is a popular implicit method, as it represents a good compromise between the advantages and disadvantages of the implicit methods. In a steady analysis, its maximum allowable Courant number is theoretically infinite, though anything more than 1000 does not make any difference to the convergence rate of a solution. The LU-SGS method can also be used as a preconditioner for the Runge-Kutta schemes to achieve a better convergence rate and stability.(Rossow, 2006).

When it comes to the harmonic balance equation system, the implementation of the LU-SGS method is quite difficult due to the fact that solutions at different time instants are connected. To reduce the programming complexity, the time spectral source term is excluded from the LU-SGS method and it is implicitly integrated using a block Jacobi method(Wang

and Huang, 2017). Although this decoupled implicit treatment of the time spectral source term can increase a solution stability, a thorough stability analysis of this numerical method has not yet been reported in the open literature.

Typically there are two main approaches for assessing the stability and convergence properties of a given numerical scheme. One is well known as the von Neumann method developed by Charney et al. (1950), which has been widely used to analyze the stability of a linear equation system with constant coefficients and periodic boundary conditions. A von Neumann analysis shows that the first-order forward temporal integration scheme is unconditionally unstable for the linearized Burger's equation in the harmonic balance form when a first-order upwind scheme is used for the spatial discretization(Hall et al., 2013). However, in practical cases where boundary conditions such as inlet, outlet, and slip wall are often applied, the stability of an equation system can improve due to the stabilization of boundary conditions. However, the effect of boundary conditions on the stability of an equation system can only be analyzed by using the matrix method or eigensystem analysis (Roberts and Swanson, 2005).

This paper presents the stability analysis results of solution methods for steady and unsteady Euler equations, for which a central scheme with blended second- and fourth-order artificial dissipation is used for the spatial discretization, and a Runge-Kutta scheme with or without implicit residual smoothing, such as the LU-SGS method and LU-SGS/BJ method, is used for time integration. Both the von Neumann and matrix methods are used to analyze the stability of the involved solution methods. Based on stability analysis results and numerical experiments, the impact of the boundary conditions and also the block Jacobi method on solution stability and convergence can be analyzed, providing insights on how to obtain a solution fast and robustly. Though the stability analysis is carried out based on the 2-D Euler equations, the conclusions can be readily extended to the 3-D RANS equations and verified in a nozzle and the NASA rotor 37 case.

## METHODOLOGY

### Flow governing equations

The unsteady Euler equations for an inviscid gas in a two dimensional Cartesian coordinate system has been used in the investigation. They are written in conservative, differential form as

$$\frac{\partial Q}{\partial t}+\frac{\partial F}{\partial x}+\frac{\partial G}{\partial y}=0 \tag{1}$$

where

$$Q=\begin{pmatrix}\rho\\ \rho u\\ \rho v\\ \rho E\end{pmatrix}, F=\begin{pmatrix}\rho u\\ \rho uu+p\\ \rho vu\\ \rho Hu\end{pmatrix}, G=\begin{pmatrix}\rho v\\ \rho uv\\ \rho vv+p\\ \rho Hv\end{pmatrix}$$

$Q$ is conservative variable vector and $F,G$ are convective flux vectors in $x$ and $y$ directions respectively. $p,\rho,u,v,E,H$ denote pressure, density, velocity components, total energy and total enthalpy. For a perfect gas

$$E=\frac{p}{(\gamma-1)\rho}+\frac{1}{2}(u^2+v^2), H=E+\frac{p}{\rho}$$

where $\gamma$ is the ratio of specific heat. The solution of Eq.(1) is obtained by using a cell-centered finite volume scheme. Spatial discretization of the equations is achieved by the well-known Jameson–Schmidt–Turkel (JST) scheme (Jameson et al., 1981) together with scalar numerical dissipation (Arnone, 1994). Then semi-discrete equations, corresponding to Eq.(1), are given by

$$\Omega\frac{\partial Q}{\partial t}+R(Q)=0 \tag{2}$$

where $\Omega$ denotes the cell volume and $R(Q)$ is the lumped sum of the spatial residual vector, containing the convective contribution $R_c(Q)$ and artificial dissipative contribution $R_d(Q)$.

### Harmonic balance method

The harmonic balance method is a computationally efficient reduced-order technique for time periodic flows within turbomachinery, particularly when compared with the dual time-stepping method (Hall et al., 2002). With the harmonic balance method, the time-dependent flow variables are approximated using a truncated temporal Fourier series

$$Q=\overline{Q}+\sum_{n=1}^{N}[Q_{A,n}\sin(\omega_n t)+Q_{B,n}\cos(\omega_n t)] \tag{3}$$

where $\overline{Q}$ is the vector of time-averaged conservative variables and $Q_{A,n},Q_{B,n}$ denote the corresponding vectors of Fourier coefficients for the $n$th harmonic with the angular frequency $\omega_n=n\omega$. For implementation, Eq.(3) can be written in a matrix form as

$$Q=DQ^* \tag{4}$$

where

$$Q = \begin{pmatrix} Q(t_1) \\ Q(t_2) \\ \vdots \\ Q(t_{2N+1}) \end{pmatrix}$$

is a larger column vector, containing the conservative variable vectors at $2N+1$ different time instants and $D$ is the discrete Fourier transform matrix, given by

$$D = \begin{pmatrix} 1 & \sin(\omega_1 t_1) & \cos(\omega_1 t_1) & \dots & \sin(\omega_N t_1) & \cos(\omega_N t_1) \\ 1 & \sin(\omega_1 t_2) & \cos(\omega_1 t_2) & \dots & \sin(\omega_N t_2) & \cos(\omega_N t_2) \\ \vdots & \vdots & \vdots & \vdots & \vdots & \vdots \\ 1 & \sin(\omega_1 t_{2N+1}) & \cos(\omega_1 t_{2N+1}) & \dots & \sin(\omega_N t_{2N+1}) & \cos(\omega_N t_{2N+1}) \end{pmatrix} \tag{5}$$

Similarly the time derivative term of the conservative variable vectors at $2N+1$ time instants can be approximated by

$$\frac{\partial Q}{\partial t} = D_t Q^* = D_t D^{-1} Q = EQ \tag{6}$$

where

$$D_t = \begin{pmatrix} 0 & \omega_1 \cos(\omega_1 t_1) & -\omega_1 \sin(\omega_1 t_1) & \dots & \omega_N \cos(\omega_N t_1) & -\omega_N \sin(\omega_N t_1) \\ 0 & \omega_1 \cos(\omega_1 t_2) & -\omega_1 \sin(\omega_1 t_2) & \dots & \omega_N \cos(\omega_N t_2) & -\omega_N \sin(\omega_N t_2) \\ \vdots & \vdots & \vdots & \vdots & \vdots & \vdots \\ 0 & \omega_1 \cos(\omega_1 t_{2N+1}) & -\omega_1 \sin(\omega_1 t_{2N+1}) & \dots & \omega_N \cos(\omega_N t_{2N+1}) & -\omega_N \sin(\omega_N t_{2N+1}) \end{pmatrix} \tag{7}$$

and the matrix $E$ is defined as the time spectral operator. Substituting Eq.(6) into Eq.(2), the harmonic balance equation system with a pseudo-time derivative term is given by

$$\Omega \frac{\partial Q}{\partial \tau} + \Omega EQ + R(Q) = 0 \tag{8}$$

where the time derivative term of the conservative variable vector in Eq.(2) is transformed into the time spectral source term $\Omega EQ$ on the left hand side of the Eq.(8) and a pseudo-time derivative term is introduced to facilitate the use of time-marching methods.

### Runge-Kutta scheme and LU-SGS method

The pseudo-time integration is accomplished through a classic four-stage Runge–Kutta scheme together with the LU-SGS method. The LU-SGS method was first proposed by Yoon and Jameson (1988) as a time integration method. It was later used as a residual smoother at each step of a Runge-Kutta scheme to improve stability and also accelerate convergence by increasing the maximum pseudo-time step (Rossow, 2006).The solution update at the $k$th stage of a Runge-Kutta scheme is defined as

$$Q^{(k)} = Q^{(0)} + \Delta Q, \quad k = 1, \dots, K \tag{9}$$

where $Q^{(0)} = Q^{n-1}$,$Q^{(K)} = Q^n$,and $\Delta Q$ is the solution increment. If the LU-SGS method is applied as a preconditioner of a Runge-Kutta method, the solution increment is obtained by solving the following equations

$$[I + \varepsilon\sigma \frac{\Delta\tau}{\Omega} \frac{\partial R}{\partial Q}]\Delta Q = -\alpha_k \sigma \frac{\Delta\tau}{\Omega} [R(Q^{(k-1)}) + \Omega E Q^{(k-1)}] \tag{10}$$

where $\varepsilon$ is the relaxation factor, $\alpha_k$ is the $k$th Runge-Kutta coefficient and $\sigma$ is the Courant number. $\Delta\tau$ is the pseudo-time step calculated based on the approximate spectral radii of the Jacobian matrix. The combination of $\varepsilon$,$\alpha_k$ and $\sigma$ plays a significant role in determining the stability and the damping behaviour of a given scheme. Typically, these coefficients should be optimized carefully by stability analysis. An approximate LU decomposition of the left hand side of Eq.(10) is given as follows

$$BLU\Delta Q = -\alpha_k \sigma \frac{\Delta\tau}{\Omega} [R(Q^{(k-1)}) + \Omega E Q^{(k-1)}] \tag{11}$$

where $L$ and $U$ are the lower and upper operators respectively and $B$ is a scalar. They are given by

$$B = 1 + \varepsilon\sigma \frac{\Delta\tau}{\Omega}(r_i + r_j)$$

$$L = 1 - \varepsilon\sigma \frac{\Delta\tau}{\Omega}(A^+_{i-1}E_i^{-1} + A^+_{j-1}E_j^{-1})/B$$

$$U = 1 + \varepsilon\sigma \frac{\Delta\tau}{\Omega}(A^-_{i+1}E_i^{+1} + A^-_{j+1}E_j^{+1})/B$$

where matrices $A^+$ and $A^-$ are defined as follows

$$A^+ = \frac{A+r}{2}, A^- = \frac{A-r}{2}$$

where $A$ is the flux Jacobian matrix of a cell face, $r$ is the spectral radius of the Jacobi matrix $A$. The shift operators $E_i^{\pm l}$ and $E_j^{\pm l}$ are defined as

$$E_i^{\pm l} Q_{i,j} = Q_{i\pm l,j}, E_j^{\pm l} Q_{i,j} = Q_{i,j\pm l}$$

More details about the derivation of the operators $BLU$ can be found in Wang and Huang (2017). As the time spectral source term in Eq.(10) is integrated explicitly, the maximum Courant number will be limited or even solution instability can occur, especially for cases with a large grid-reduced frequency.

### Block Jacobi method

In order to mitigate the impaired solution stability caused by the time spectral source term, it need be integrated implicitly together with other terms as follows

$$[I + \varepsilon\sigma\frac{\Delta\tau}{\Omega}(\frac{\partial R}{\partial Q} + \Omega E)]\Delta Q = -\alpha_k\sigma\frac{\Delta\tau}{\Omega}[R(Q^{(k-1)}) + \Omega E Q^{(k-1)}] \tag{12}$$

However, the exact inversion of the system Jacobian matrix of $I + \varepsilon\sigma\frac{\Delta\tau}{\Omega}(\frac{\partial R}{\partial Q} + \Omega E)$ is quite complicated, as $E$ is a dense matrix and depends on all time instants. To avoid this complexity, the block Jacobi method was proposed by Sicot et al. (2008) to approximately invert the Jacobian matrix of the time spectral source term through iterations. The integration of the LU-SGS method and the block Jacobi method is given as follows

$$BLU\Delta Q^m = -\alpha_k\sigma\frac{\Delta\tau}{\Omega}[R(Q^{k-1}) + \Omega E Q^{(k-1)}] + \Omega E\Delta Q^{m-1} \tag{13}$$

where $m$ is the block Jacobi iteration index. When $m$ equals 1, $\Delta Q^0 = 0$. At least two Jacobi iterations are required to have the time spectral source term integrated implicitly. The advantage of the block Jacobi method is its easy implementation and minimal alterations to existing codes with a baseline LU-SGS method.

When using the LU-SGS/BJ method to solve the harmonic balance equation system, one important thing to remember is that the scalar $B$ in Eq.(11) must account for the influence of the time spectral source term on the spectral radius of the system Jacobian matrix, otherwise the solution of harmonic balance equation system will become unstable. To prevent this, the scalar $B$ can be modified as follows

$$B = 1 + \varepsilon\sigma\frac{\Delta\tau}{\Omega}(r_i + r_j + N\Omega\omega)$$

### Boundary conditions

In general, there are four kinds of boundary conditions used in stability analysis: subsonic inlet, subsonic outlet, slip wall and periodic boundary conditions. At a subsonic inlet, the total pressure, total temperature and flow angle are specified. Static pressure can be extrapolated from the interior domain to the boundary. One can also extrapolate the one-dimensional Riemann invariant to the inlet boundary.

$$R^- = V - \frac{2c}{\gamma - 1} \tag{14}$$

where $R^-$ is the Riemann invariant, $V$ is the flow velocity, $c$ is the speed of sound. Well-posedness of a boundary condition is important for a numerical analysis as it can affect solution convergence characteristics and even solution accuracy. Extrapolating the Riemann invariation at an inlet boundary has been found to offer better convergence properties for nozzle flows (Jameson and Caughey, 2001). Nevertheless, there is no stability analysis to support this conclusion. This paper will examine the better convergence characteristics of extrapolating the Riemann invariant by stability analysis.

For a subsonic outlet boundary condition, the static pressure is specified. In order to obtain a meaningful unsteady solution for a Laval nozzle and the NASA rotor 37 using the harmonic balance method, a sinusoidal static pressure is prescribed

$$p = \overline{p} + \Delta p sin(\omega t) \tag{15}$$

where $\overline{p}$ is the time-averaged static pressure, which is also used for obtaining a steady solution. $\Delta p$ is the amplitude of static pressure perturbation with the value $\Delta p = 0.1\overline{p}$ in our work. $\omega$ is the angular frequency of unsteadiness.

### von Neumann method

Though Swanson et al. (2007) performed a stability analysis of the RK/LU-SGS methods for two dimensional steady Euler equations, there has been no such effort of the RK/LU-SGS methods for solving the harmonic balance equation system in the open literature. The stability and damping behaviors of the RK/LU-SGS methods will change dramatically due to the time spectral source term in unsteady Euler equations with the harmonic balance method being used. To improve the solution stability of a harmonic balance equation system, the block Jacobi method is often used. Therefore, there is also a need to perform a stability analysis of the RK/LU-SGS/BJ method for solving the harmonic balance equation system.

In the von Neumann analysis, we assume the Euler equations are solved in a finite domain with periodic boundary conditions. So the numerical error, which has the same form as the solution, can be decomposed into spatial Fourier series.

$$Q_{i,j} = \sum_{n=-i_m}^{i_m} \sum_{m=-j_m}^{j_m} \hat{Q}_{n,m} e^{[J(i\varphi_x + j\varphi_y)]} \tag{16}$$

where $J = \sqrt{-1}$ is the imaginary unit, $\hat{Q}_{n,m}$ is the amplitude of the spatial harmonic, as well as $\varphi_x$ and $\varphi_y$ are the phase angles, covering the domain of $[-\pi, \pi]$. Let us define a Cartesian grid consisting of $i_m \times j_m$ cells, where the length and width of each cell are denoted by $\Delta x$ and $\Delta y$, respectively. $Q_{i,j}$ represents the numerical error that arises from numerical truncation and an inappropriate initial flow filed.

The von Neumann analysis can only be applied to a linear equation system, however, Eq.(13) is obviously a non-linear equation. To make the formulation linear, a local stability analysis is required with the non-linear term being frozen at certain values. The semi-discrete harmonic balance equation system Eq.(13) can be linearized as

$$BLU\Delta Q^m_{i,j} = -\alpha_k \sigma \frac{\Delta\tau}{\Omega}[\mathscr{L} + \Omega E]Q^{(k-1)}_{i,j} + \Omega E \Delta Q^{m-1}_{i,j} \tag{17}$$

where $\mathscr{L}$ is the linearized discrete residual operator defined by

$$\mathscr{L} = \mathscr{L}_c + \mathscr{L}_d \tag{18}$$

consisting of the convective part $\mathscr{L}_c$ and dissipative part $\mathscr{L}_d$. In the von Neumann analysis, the grid uniformities is assumed. Thus $\mathscr{L}_c$ and $\mathscr{L}_d$ can be given simply by

$$\begin{aligned}
\mathscr{L}_c =& \frac{\Delta y}{2}[J_A(E_i^{+1} - E_i^{-1})] + \frac{\Delta x}{2}[J_B(E_j^{+1} - E_j^{-1})] \\
\mathscr{L}_d =& \Lambda_i \varepsilon^{(4)}[E_i^{+2} - 4E_i^{+1} + 6 - 4E_i^{-1} + E_i^{-2}] \\
& \Lambda_j \varepsilon^{(4)}[E_j^{+2} - 4E_j^{+1} + 6 - 4E_j^{-1} + E_j^{-2}]
\end{aligned}$$

with $J_A$ and $J_B$ becoming the flux Jacobian matrices ,$\Lambda_i$ and $\Lambda_j$ becoming the eigenvalues of the flux Jacobian matrices. Put the discrete Fourier transform Eq.(16) into Eq.(17), we can obtain

$$B\hat{L}\hat{U}\Delta\hat{Q}^m = -\alpha_k \sigma \frac{\Delta\tau}{\Omega}[\hat{\mathscr{L}} + \Omega E]\hat{Q}^{(k-1)} + \Omega E \Delta\hat{Q}^{m-1}_{i,j} \tag{19}$$

where the transformed linear residual operator $\hat{\mathscr{L}}$ is the function of phase angle of $\varphi_x$ and $\varphi_y$, given by

$$\hat{\mathscr{L}} = \hat{\mathscr{L}}_c + \hat{\mathscr{L}}_d \tag{20}$$

where

$$\begin{aligned}
\hat{\mathscr{L}}_c =& \frac{\Delta y}{2}[J_A(e^{J\varphi_x} - e^{-J\varphi_x})] + \frac{\Delta x}{2}[J_B(e^{J\varphi_y} - e^{-J\varphi_y})] \\
\hat{\mathscr{L}}_d =& \Lambda_i \varepsilon^{(4)}[e^{2J\varphi_x} - 4e^{J\varphi_x} + 6 - 4e^{-J\varphi_x} + e^{-2J\varphi_x}] \\
& + \Lambda_j \varepsilon^{(4)}[e^{2J\varphi_y} - 4e^{J\varphi_y} + 6 - 4e^{-J\varphi_y} + e^{-2J\varphi_y}]
\end{aligned}$$

$\hat{L}$ and $\hat{U}$ are the transformed lower and upper operators, given by

$$\begin{aligned}
\hat{L} &= 1 - \varepsilon\sigma \frac{\Delta\tau}{\Omega}(\Delta y J_A^+ e^{-J\varphi_x} + \Delta x J_B^+ e^{-J\varphi_y})/B \\
\hat{U} &= 1 + \varepsilon\sigma \frac{\Delta\tau}{\Omega}(\Delta y J_A^- e^{J\varphi_x} + \Delta x J_B^- e^{J\varphi_y})/B
\end{aligned}$$

The transformed increment of the solution with the block Jacobi iteration index $m$ can be simplified as

$$\Delta\hat{Q}^m = -\alpha_k \sigma \frac{\Delta\tau}{\Omega}\hat{P}^m[\hat{\mathscr{L}} + \Omega E]\hat{Q}^{(k-1)} \quad m = 1, 2, \ldots \tag{21}$$

where the preconditioner of the LU-SGS method and the block Jacobi method $P^m$ is given by

$$\begin{cases} \hat{P}^m = (B\hat{L}\hat{U})^{-1} & m = 1 \\ \hat{P}^m = \hat{P}^1(1 - \varepsilon\sigma\frac{\Delta\tau}{\Omega}\Omega E\hat{P}^{m-1}) & m = 2,3,\ldots \end{cases}$$

When $m = 1$ the LU-SGS method is applied only, while when $m \geq 2$ the block Jacobi method is implemented to deal with the time spectral source term implicitly. As the $K$-stage Runge-Kutta method is used for pseudo-time integration, the updated numerical error in the next pseudo-time step can be written as

$$\hat{Q}^n = G_{RK}\hat{Q}^{n-1} \tag{22}$$

where the amplification factor matrix $G_{RK}$ is given by

$$G_{RK} = I + \sum_{k=1}^{K} \alpha_K \ldots \alpha_{K-k+1} Z^k \tag{23}$$

in which $I$ is the identity matrix and $Z$ is the Fourier symbol of the spatial operator, defined by

$$Z = -\sigma\frac{\Delta\tau}{\Omega}\hat{P}^m[\hat{\mathscr{L}} + \Omega E] \tag{24}$$

which is a function of the phase angles $\varphi_x$ and $\varphi_y$ and the Courant number $\sigma$. The Courant number acts as a scale factor of the Fourier symbol. When the Runge-Kutta coefficients in Eq.(23) are specified, the amplification factor matrix is only determined by the Fourier symbol $Z$. The amplification factor measures the growth of the numerical error over iteration. For a stably scheme, the numerical error must not grow with iteration. So the modulus of amplification factor $|G_{RK}|$ must be less than or equal to one for the all phase angles $\varphi_x$ and $\varphi_y$ varying from $[-\pi, \pi]$. In other words, the locus of the Fourier symbol $Z$ in the complex plane, when phase angles vary, should be inside the stability region of the time integration method. The allowable Courant number thus depends on the interval between the locus of the Fourier symbol and stability domain along the imaginary axis as well as the negative real axis.

### Matrix method

Matrix method, also known as eigenvalue analysis, is a more general approach for stability analysis. It can take into account the influence of boundary conditions, grid nonuniformities and flow filed nonuniformities. In the case of a non-uniform mesh, the total residual function $R(Q)$ for each control volume consists of two part: the convective part $R_c(Q)$ and the artificial dissipative part $R_d(Q)$. They are expressed as follows

$$\begin{aligned} R_c(Q) =& [F_{con,i+\frac{1}{2},j} - F_{con,i-\frac{1}{2},j}] + [F_{con,i,j+\frac{1}{2}} - F_{con,i,j-\frac{1}{2}}] \\ R_d(Q) =& [D_{i+\frac{1}{2},j} - D_{i-\frac{1}{2},j}] + [D_{i,j+\frac{1}{2}} - D_{i,j-\frac{1}{2},j}] \end{aligned} \tag{25}$$

where the convective fluxes in surface with the index $i + \frac{1}{2}$, omitting the index $j$, is defined by

$$F_{con,i+\frac{1}{2}} = [F \times S_x + G \times S_y]_{i+\frac{1}{2}} \tag{26}$$

where $S_x$ and $S_y$ are the bounding surface projections in the two coordinate directions. Fluxes at a bounding surface are calculated by simply averaging their values on two sides of the bounding surface. For example, $F_{i+\frac{1}{2}} = \frac{1}{2}(F_i + F_{i+1})$. The artificial dissipative fluxes are given by

$$D_{i+\frac{1}{2}} = \Lambda_{i+\frac{1}{2}}\varepsilon^{(2)}_{i+\frac{1}{2}}(Q_{i+1} - U_i) - \varepsilon^{(4)}_{i+\frac{1}{2}}(Q_{i+2} - 3Q_{i+1} + 3Q_i - Q_{i-1}) \tag{27}$$

where there are both nonlinear and linear dissipative terms with the coefficients $\varepsilon^{(2)}$ and $\varepsilon^{(4)}$. The nonlinear term is designed to provide dissipation at discontinuities, for example, the shock wave. And the linear one is used to suppress spurious solutions, leading a fast convergence to the steady state. The coefficients $\varepsilon^{(2)}$ and $\varepsilon^{(4)}$ depend on the distribution of static pressure from the solution and the constant parameters $k^{(2)}$ and $k^{(4)}$(Jameson et al., 1981).

The semi-discrete equations, shown in Eq.(11), can be rewritten in a matrix form as

$$\boldsymbol{BLU}\Delta\boldsymbol{Q} = -\alpha_k\sigma\boldsymbol{dtv}[\boldsymbol{R}(\boldsymbol{Q}^{(k-1)}) + \boldsymbol{\Omega E}\boldsymbol{Q}^{(k-1)}] \tag{28}$$

where $\boldsymbol{BLU}$ is the implicit operator matrix and $\boldsymbol{R}(\boldsymbol{Q}^{(k-1)})$ is the discrete residual vector containing the convective fluxes and dissipative fluxes at the each cell under various boundary conditions. $\boldsymbol{Q}$ is the solution vector containing the conservative

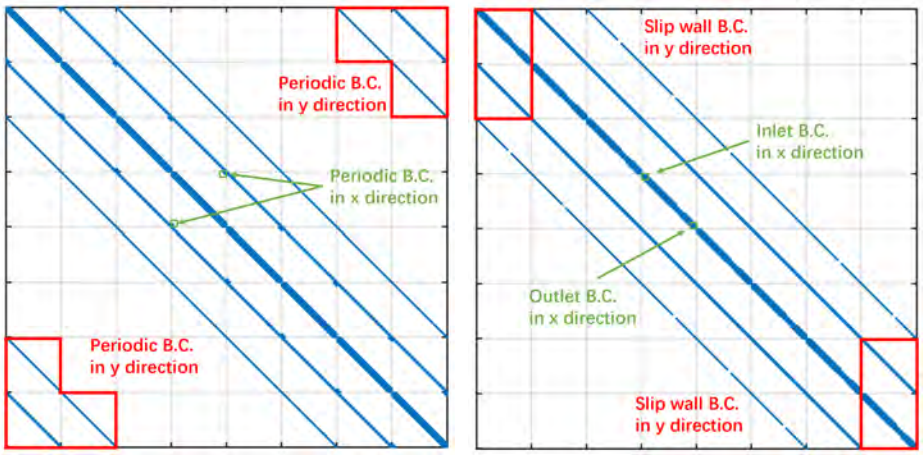


(a) Periodic B.C. in x and y directions

(b) Inlet,outlet B.C. in x direction and slip wall B.C. in y direction

**Figure 1 The Jacobian matrix of spatial discrete operator for 2-D Euler equation system. Nonzero elements displayed as filled blue dots.**

variables at each cell, given by

$$\boldsymbol{Q} = \begin{Bmatrix} Q_{1,1} \\ Q_{2,1} \\ \vdots \\ Q_{i_m,1} \\ Q_{1,2} \\ \vdots \\ Q_{i_m,j_m} \end{Bmatrix} \tag{29}$$

and $\boldsymbol{dtv}$,$\boldsymbol{\Omega E}$ are diagonal matrices which contain the ratios of pseudo-time step to volume and time spectral source terms at each cell. Then the large nonlinear equation system is linearized as

$$\Delta \boldsymbol{Q} = -\alpha_k \sigma \boldsymbol{dtv} \boldsymbol{P} [\boldsymbol{C} + \boldsymbol{\Omega E}] \boldsymbol{Q}^{(k-1)} \tag{30}$$

where $\boldsymbol{C} = \frac{\partial \boldsymbol{R}}{\partial \boldsymbol{Q}}$ is the Jacobian matrix of spatial discretization operator, which have been derived manually in the Appendix, and $\boldsymbol{P}$ is the preconditioner matrix. The Jacobian matrix $\boldsymbol{C}$ and the preconditioner matrix $\boldsymbol{P}$ are usually frozen with a initial or fully convergent steady solution. Different boundary conditions, such as inlet, outlet and slip wall, are considered in the stability analysis though altering the submatrix of the Jacobian matrix $\boldsymbol{C}$ as shown in Fig.1.

After the Jacobian matrix $\boldsymbol{C}$ has been assembled, the amplification factor matrix of the equation system, integrated by the Runge-Kutta method, is given by

$$\boldsymbol{G}_{RK} = \boldsymbol{I} + \sum_{k=1}^{K} \alpha_K \dots \alpha_{K-k+1} \boldsymbol{Z}^k \tag{31}$$

where the transform matrix is defined as

$$\boldsymbol{Z} = -\sigma \boldsymbol{dtv} \boldsymbol{P} [\boldsymbol{C} + \boldsymbol{\Omega E}] \tag{32}$$

The dimension of the matrix $\boldsymbol{G}_{RK}$ is $n_{nvar} \times i_m \times j_m \times (2N+1)$, where $n_{var}$ is the number of conservative variable(4 for two dimensional Euler equations), $i_m$ and $j_m$ is the number of control volume in $x$ and $y$ direction respectively and $N$ is the number of harmonics. So the total number of eigenvalues of the amplification factor matrix $\boldsymbol{G}_{RK}$ is equal to $n_{nvar} \times i_m \times j_m \times (2N+1)$. The time-stepping scheme will be linearly stable, if all of the modulus of these eigenvalues are less than one.

## RESULTS AND DISCUSSION

This section shows two different case studies. The first case is aimed at investigating the stability of the explicit Runge-Kutta methods with the JST scheme in the harmonic balance equation system by both the von Neumann method. The stability of these schemes are also analyzed by the matrix method to consider the impact of various boundary conditions. The second case focuses on the stability analysis of the LU-SGS method in the time spectral form 2-D Euler equations and also the stabilization of the block Jacobi method with different grid-reduced frequencies.

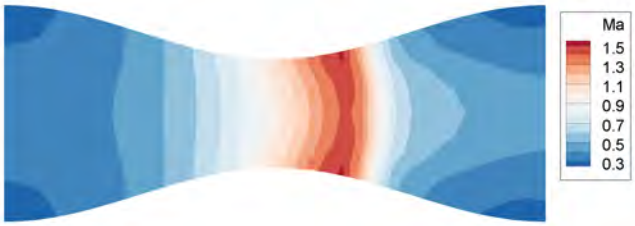


**Figure 2 The Mach number contours of Laval nozzle solved with 2-D steady Euler equations**

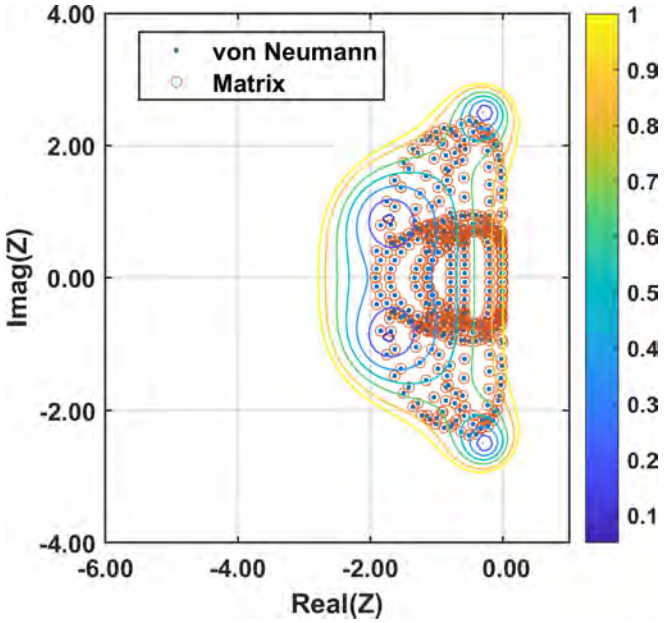


**Figure 3 The locus of the Fourier symbol and the eigenvalue spectrum of the transform matrix with periodic boundary conditions, uniform flow fields and grids($AR = 0.625, Ma = 0.5, \beta = 0°, k^{(4)} = 0.21, \sigma = 3$) and the contours of the magnitude of the amplification factor in the case of the classic four-stage Runge-Kutta scheme.**

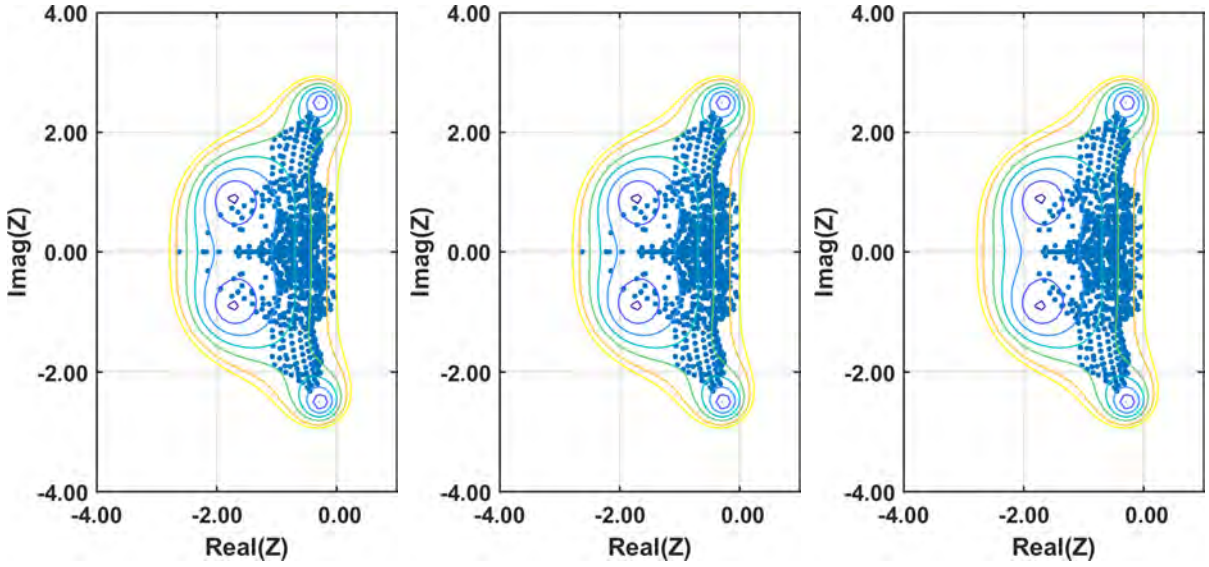


**(a) Inlet1,$k^{(2)} = 0.0$** **(b) Inlet1,$k^{(2)} = 0.5$** **(c) Inlet2,$k^{(2)} = 0.5$**

**Figure 4 The eigenvalue spectrum of the transform matrix with the baseline of the nozzle flow with different boundary conditions and the second order artificial coefficient $k^{(2)}$( $k^{(4)} = 0.021, \sigma = 3$).**

**Case1: The stability of explicit Runge-Kutta scheme for different boundary conditions**

At the start of this case, the stability of explicit Runge-Kutta schemes in steady Euler equations with periodic boundary conditions was studied. The solution of the equations was solved in a two dimensional, rectangular and uniform mesh with 33 grid points in the $x$ direction and 8 grid points in $y$ direction, resulting the aspect ratio $AR = 0.625$. The uniform flow filed with the Mach number $Ma = 0.5$ and the flow angle $\beta = 0°$, was used as a baseline for linearization. The stability in this situation was analyzed and compared by the von Neumann method and the matrix method. The time spectral source term is equal to 0 due to the basic angular frequency $\omega = 0$ in steady flow. Fig.3 demonstrates that the locus of the Fourier symbol $Z$ obtained by the von Neumann analysis and the distribution of eigenvalues of the transform matrix $\boldsymbol{Z}$ obtain by the matrix method are identically consistent, resulting the same damping behaviour and the maximum allowable Courant number. The contours of the amplification factor magnitude of the classic four-stage Runge-Kutta scheme with coefficients $\alpha = [1/4, 1/3, 1/2, 1]$ are also shown in Fig.3. The contour levels is given as $|G| = 0.002, 0.01, 0.05, 0.20, 0.35, 0.50, 0.65, 0.85, 1.00$. The outermost contour represents the magnitude of the amplification factor is equal to 1. The locus of the Fourier symbol for all phase angles or the distribution of the eigenvalues of the transform matrix must lie within the stability domain to ensure the maximum magnitude of the amplification factor not large than 1, so that the solution can converge.

In the next step, the influence of different boundary conditions and nonlinear artificial dissipative term were taken into consideration by matrix method. The steady solution of the nozzle case, with the same number of grids as the rectangular mesh, is shown in Fig.2, which was used as baseline of linearization for matrix stability analysis. As we can see, there is a shock wave near the throat with the maximum Much number $Ma = 1.5$, representing a strong non-linearity in the solution. The introduction of the slip wall, the subsonic inlet and outlet boundary conditions in a 2-D Laval nozzle case leads to significant changes in the eigenvalue distribution, shown in Fig.4a. The static pressure is extrapolated at the inlet , defined as $inlet1$. Then the second order artificial dissipation is considered with $k^{(2)} = 0.5$, causing slightly different eigenvalue distribution, shown in Fig.4b. Finally the second type of subsonic inlet boundary condition with Riemann invariant extrapolation is implemented. In Fig.4c, the eigenvalues alone the real axis in negative direction collapse away from the stability boundary leading to the better stability and the damping property.

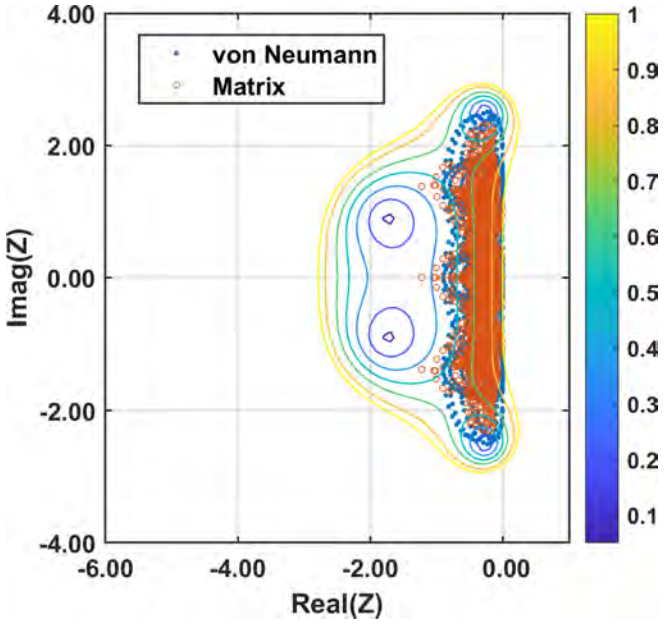


**Figure 5 The locus of Fourier symbol and the eigenvalue spectrum of the transform matrix($\omega_x = 1, \sigma = 1.4$) and the contours of the magnitude of the amplification in the case of the classic four-stage Runge-Kutta scheme**

To asses the stability of harmonic balance equation system, the eigenvalues of time spectral source term were counted when $\omega > 0$. In the stability analysis, the time spectral source term introduces a pure imaginary part into the Fourier symbol in the von Neumann analysis and also into the eigenvalues of the transform matrix in the matrix analysis, leading a shift alone the imaginary axis in the complex plane, shown in Fig.5. The degree of shifting is related with the unsteady angular frequency, number of harmonic, grid size and also the eigenvalue of Jacobian matrix of flux vector. A dimensionless parameter, the maximum grid-reduced frequency, is defined as

$$\omega_x = \frac{N\omega\Omega}{\lambda_x + \lambda_y} \tag{33}$$

where $\lambda_x$ and $\lambda_y$ are the maximum eigenvalue of Jacobi matrix of convective fluxes in $x$ and $y$ directions respectively.

$N$ is the number of harmonic. $\omega$ is the angular frequency of the unsteadiness and $\Omega$ is the cell volume. The maximum grid-reduced frequency is an critical parameter that has a substantial impact on the stability analysis for harmonic balance equation system. If the maximum grid-reduced frequency exceeds a certain value, the resulting locus of the Fourier Symbol or the distribution of the eigenvalues will shift outside the stability region. at this time, a smaller Courant number must be limited to scale down the spectrum of the spatial discretization operator inside the stability domain.

The numerical experiments were implemented in our in-house solver to verify the result obtained by the stability analysis, shown in Fig.6. As the maximum grid-reduced frequency increases, the maximum allowable Courant number decreases due to the shift of the eigenvalues. The phenomena are observed in both two different inlet subsonic boundary conditions analyzed by matrix method and periodic boundary conditions analyzed by von Neumann method, as illustrated in Fig.6. *Inlet*1 represents the subsonic inlet boundary that the statistic pressure is extrapolated and *Inlet*2 represents the inlet boundary with an extrapolation of Riemann invariant. As we can see, the maximum Courant number of *inlet*2 is higher than that of *inlet*1 due the clustering of the eigenvalue, especially along the negative real axis, of course is also larger than that of periodic boundary analyzed by von Neumann method. The actual maximum Courant numbers obtained by numerical experiments, are in good agreement with the theoretical predictions of stability analysis.

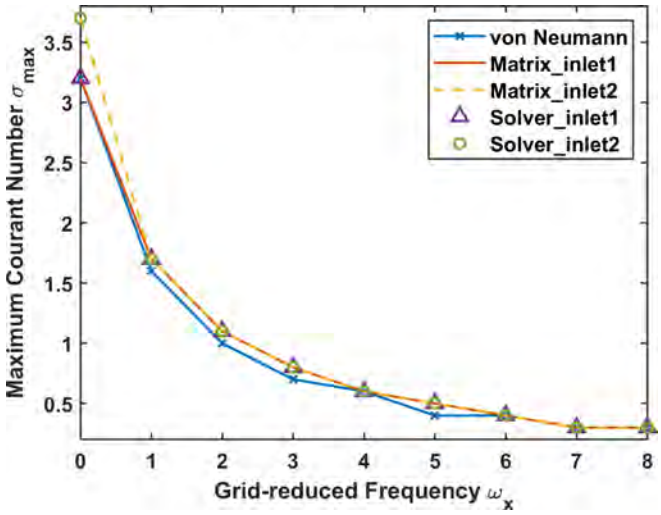


**Figure 6 The maximum Courant number varying with the maximum grid-reduced frequency**

### Case2: the stability of the LU-SGS method with the block Jacobi method

The second case demonstrates the stability properties of the LU-SGS method in the harmonic balance equation system and also the stabilization effect of the block Jacobi method. In this case, the NASA rotor 37 was employed as a more practical example to verify the stability analysis in turbomachinery. The 3-D RANS equations with the SA turbulence model were solved with a slip wall boundary condition and using the wall function in our in-house solver, TurboXD. Similar to the first nozzle case, the frequency of the unsteadiness depended on the perturbation of back pressure at the outlet of the passage between the two blades. In this analysis, there was an H mesh with 57 grid points in the radial direction and 49 grid points in the circumferential direction and 137 grid points in the streamwise direction, among which 72 grid points were on the blade surface. The Mach number contours of the steady solution is shown in Fig.7. As observed, the flow in the passage exhibits transonic behavior characterized by the presence of a shock wave, with a maximum Mach number of approximately 1.5.

The 2-D Euler equation system with the time spectral source term instead of the 3-D RANS equations for simplification was used to implement the stability analysis. In this case, the LU-SGS method with the block Jacobi method, used as a preconditioner for an explicit Runge-Kutta method, was taken into consideration in the stability analysis. Firstly, for the steady Euler equation system solved by the LU-SGS method, there is a kidney-shape locus of the Fourier symbol in the complex plane, quite different from the explicit one, covered by the stability domain of the four-stage Runge-Kutta scheme, even when Courant number increases to the order of $10^3$. In this case, the LU-SGS method provides a significant improvement in stability compared with the explicit method, so that a large allowable Courant number can be achieved to increase the convergence rate. However, it is important to note that the cost of each iteration with the LU-SGS method is higher than that of the explicit method.

For the unsteady Euler equation system with the time spectral source term, the locus of the Fourier symbol moves toward the imaginary axis when the maximum grid-reduced frequency increases from 0 to 0.1, as shown in Fig.8b. When the maximum grid-reduced frequency reaches 0.5 in Fig.8c, the Fourier symbols extend behind the stability boundary of the classic four-stage Runge-Kutta scheme, Consequently leading the magnitude of amplification factor larger than unity. Then the block Jacobi method was used to deal with the time spectral source term implicitly. As we can see in Fig.8c, the

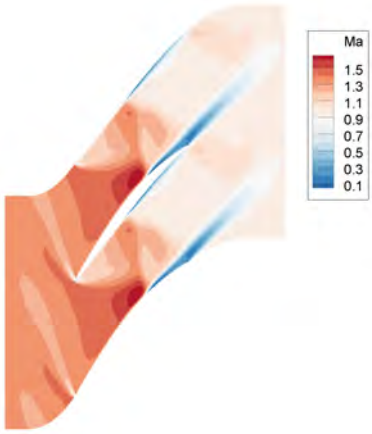


**Figure 7 The Mach number contours of the NASA rotor 37 solved with steady 3-D RANS equations**

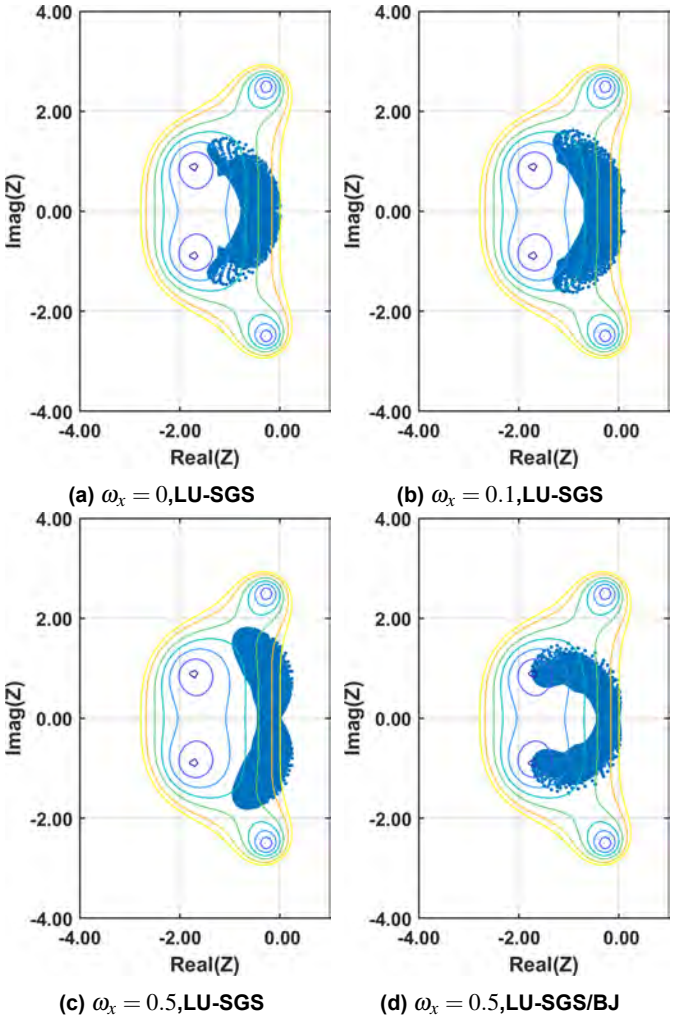


**(a)** $\omega_x = 0$**,LU-SGS** **(b)** $\omega_x = 0.1$**,LU-SGS**

**(c)** $\omega_x = 0.5$**,LU-SGS** **(d)** $\omega_x = 0.5$**,LU-SGS/BJ**

**Figure 8 The locus of the Fourier symbol with different values of the maximum grid-reduced frequency(**$\sigma = 1000, \varepsilon = 0.5$**) and the contours of the magnitude of the amplification factor in the case of classic four-stage Runge-Kutta scheme**

Fourier symbol locus clusters within the stability domain again for the maximum grid-reduced frequency $\omega_x = 0.5$. As a result, the block Jacobi method can stabilize the solution by constraining the locus of the Fourier Symbol away from the imaginary axis back into the stability domain.

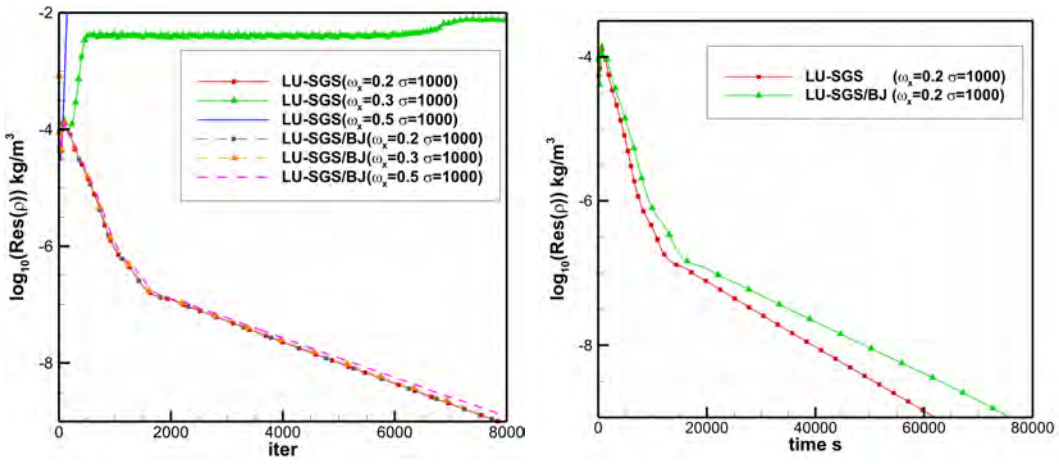


(a) iteration (b) CPU time

**Figure 9 The convergence history of Res($\rho$) solved with using the LU-SGS method and the LU-SGS/BJ method($\varepsilon = 0.6$)**

The numerical experiments were conducted to verify the stability results analyzed through the von Neumann method. In Fig.9a, both the LU-SGS and the LU-SGS/BJ method can achieve good convergent solutions when the maximum grid-reduced frequency is less than 0.2. However, when the maximum grid-reduced frequency exceeds 0.2, the LU-SGS method fails to achieve convergent solutions with the constant Courant number $\sigma = 1000$ and relaxation factor $\varepsilon = 0.6$. Conversely, the LU-SGS/BJ method can obtain solutions that converge effectively. Fig.9b illustrates the time cost comparison between the LU-SGS method and LU-SGS/BJ method. As expected, the LU-SGS method with the block Jacobi method requires more CPU time per iteration than the LU-SGS method alone. Based on the analysis, we suggest that the block Jacobi method is unnecessary when the maximum grid-reduced frequency is below 0.2. However, if the maximum grid-reduced frequency exceeds this value, the time spectral source term will compromise the stability of the equation system. In such cases, it is recommended to use the block Jacobi method to stabilize the solution and allow for a larger Courant number.

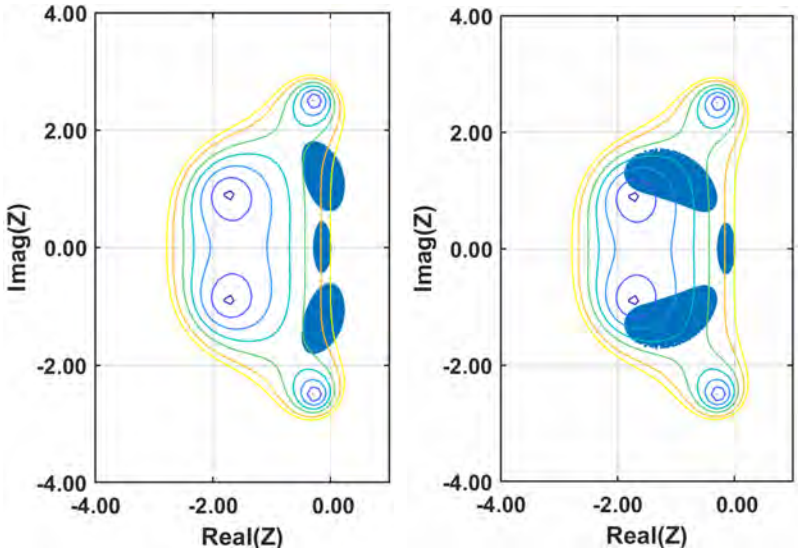


(a) The LU-SGS method only (b) The LU-SGS method with the block Jacobi method

**Figure 10 The locus of the Fourier symbol($\omega_x = 2, \sigma = 1000, \varepsilon = 0.6$).**

Furthermore, when the maximum grid-reduced frequency is big enough, the time spectral source term will causes significant stability issue, if the LU-SGS method is utilized alone without the block Jacobi method. In Fig.10a, the Fourier symbol locus lies outside of the stability domain when $\omega_x = 2$ and $\sigma = 1000$. Then the block Jacobi method is used to

restrict the locus inside the stability domain and stabilize the solution, as shown in Fig.10b. The corresponding numerical experiments were conducted to verify the stability analysis results as shown in Fig.11a. It can be seen that the solution solved with the LU-SGS method can only converge with a very low Courant number, approximately equal to 1. However with the LU-SGS/BJ method, the maximum Courant number can reach up to 1000, even higher, resulting in a good convergence rate. In terms of the total CPU time, less time cost is required by LU-SGS/BJ method to achieve convergence, approximately 23.5% of that required by the LU-SGS method, when the residual level of density reach $10^{-7}$. This acceleration mainly due to much higher Courant number that the LU-SGS/BJ method can achieve to let the solution converge. For the more practical problems in turbomachinery by solving the RANS equations with a finer mesh of NASA rotor 37, the total number of which is twice that of the coarse mesh, the convergence performance of the LU-SGS/BJ method still keep, shown in Fig.11b. Notably, the maximum grid-reduced frequency experiences a reduction due to the decrease in cell volume associated with the finer mesh. However the LU-SGS method exhibits the worse convergence performance due to the increased grid numbers.

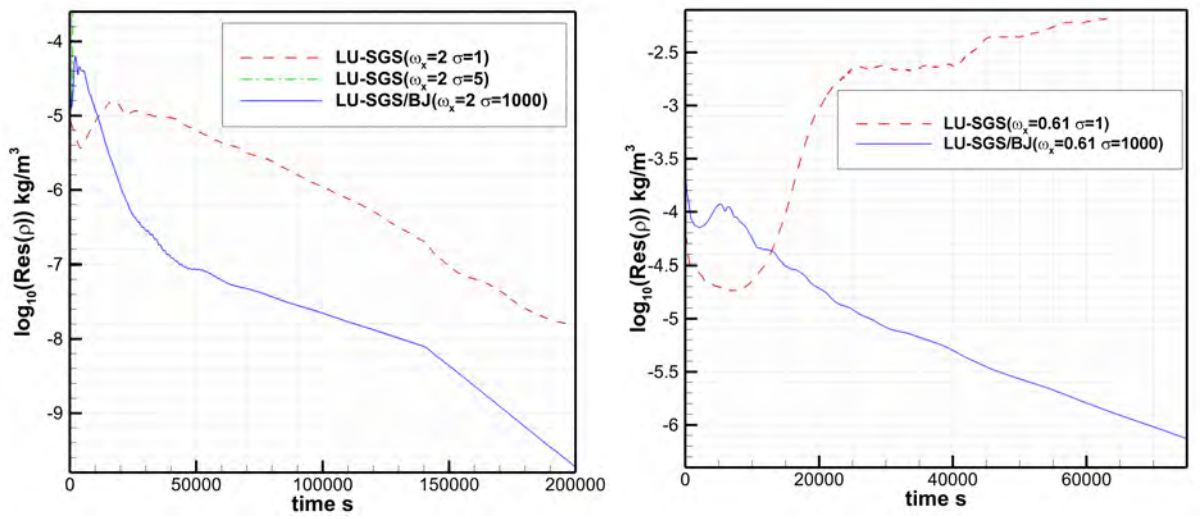


**(a) Coarse mesh** **(b) Fine mesh**

**Figure 11 The convergence history of Res($\rho$) with using the LU-SGS method and the LU-SGS/BJ method($\varepsilon = 0.6$).**

## CONCLUSION

In this work, we have investigated the stability of an explicit Runge-Kutta time integration with the JST spatial discretization scheme, using the LU-SGS method alone with the block Jacobi method as a preconditioner, in a 2-D Euler harmonic balance equation system. For periodic boundary conditions, both the von Neumann method and the matrix method showed identical stability analysis results that an explicit four-stage Runge-Kutta method without preconditioners is conditional stable for the time spectral form Euler equations. However with the boundary conditions such as, inlet, outlet and slip wall boundary conditions, often used in practical cases, the eigenvalue spectrum of the transform matrix could change dramatically, leading a significant influence on the stability and damping properties. Furthermore, the matrix stability analysis revealed that using the Riemann invariant extrapolation at an inlet can improve the stability though clusteing the eigenvalues alone the negative real axis away from the stability boundary.

As mentioned in Gentilli (2010), the maximum Courant number decreases significantly with the increasing maximum grid-reduced frequency. Our von Neumann analysis demonstrated that the introduction of time spectral source term leads a shift along the imaginary axis in the Fourier symbol locus. Consequently the Fourier symbol locus more easily extend behind the stability boundary along the imaginery axis, causing a smaller allowable Courant number. The extent of the shift, which is also measured as the stiffness, is contingent upon the value of the maximum grid-reduced frequency. In order to mitigate the impaired solution stability caused by the stiffness of the time spectral source term, the LU-SGS/BJ method, as a preconditioner of an explicit Runge-Kutta method, was used and analyzed. In our von Neumann stability analysis, the stiffness associated with the time spectral source term is addressed by the block Jacobi method so that a theoretically infinite Courant number can be achieved for an appropriate combination of Runge-Kutta coefficients and relaxation factor in LU-SGS method. Nevertheless, the implementation of the block Jacobi method introduces additional computational costs. To balance stability and computational efficiency, we suggest that when the maximum grid-reduced frequency $\omega_x \leq 0.2$, using the LU-SGS method alone is sufficient to ensure stability and save the computational effort for solving the harmonic balance equation system, as the stiffness caused by the time spectral source term is negligible. However for a large unsteady frequency with $\omega_x > 0.2$, the utilization of the block Jacobi method becomes necessary to enable a Courant number of 1000 to achieve a great convergence rate; Otherwise, a very low Courant number of approximately 1 must be enfored to maintain

stability.


## ACKNOWLEDGMENTS

The work is supported by Science Center for Gas Turbine Project (Project No. P2022-C-II-001-001)


## REFERENCES


Arnone, A. (1994), 'Viscous analysis of three-dimensional rotor flow using a multigrid method', *Journal of Turbomachinery* **116**(3), 435–445.
**URL:** *https://doi.org/10.1115/1.2929430*

Charney, J. G., Fjörtoft, R. and von Neumann, J. (1950), 'Numerical integration of the barotropic vorticity equation', *Tellus* **2**(4), 237–254.
**URL:** *https://doi.org/10.3402/tellusa.v2i4.8607*

Gentilli, N. C. (2010), Efficient Solution of Unsteady Nonlinear Flows Using a Multiple Zone Harmonic Balance Technique, PhD thesis, Duke University.

Hall, K. C., Ekici, K., Thomas, J. P. and Dowell, E. H. (2013), 'Harmonic balance methods applied to computational fluid dynamics problems', *International Journal of Computational Fluid Dynamics* **27**(2), 52–67.
**URL:** *https://doi.org/10.1080/10618562.2012.742512*

Hall, K. C., Thomas, J. P. and Clark, W. S. (2002), 'Computation of unsteady nonlinear flows in cascades using a harmonic balance technique', *AIAA Journal* **40**(5), 879–886.
**URL:** *https://doi.org/10.2514/2.1754*

Jameson, A. and Caughey, D. (2001), 'How many steps are required to solve the Euler equations of steady, compressible flow-in search of a fast solution algorithm', AIAA Paper, 2001–2673.
**URL:** *https://doi.org/10.2514/6.2001-2673*

Jameson, A., Schmidt, W. and Turkel, E. (1981), 'Solutions of the Euler equations by finite volume methods using Runge-Kutta time-stepping schemes', AIAA Paper, 81–1259.
**URL:** *https://doi.org/10.2514/6.1981-1259*

Roberts, T. and Swanson, R. (2005), 'A study of multigrid preconditioners using eigensystem analysis', AIAA Paper, 2005–5229.
**URL:** *https://doi.org/10.2514/6.2005-5229*

Rossow, C.-C. (2006), 'Convergence acceleration for solving the compressible Navier-Stokes equations', *AIAA Journal* **44**(2), 345–352.
**URL:** *https://doi.org/10.2514/1.15636*

Sicot, F., Puigt, G. and Montagnac, M. (2008), 'Block-Jacobi implicit algorithms for the time spectral method', *AIAA Journal* **46**(12), 3080–3089.
**URL:** *https://doi.org/10.2514/1.36792*

Swanson, R. C., Turkel, E. and Rossow, C.-C. (2007), 'Convergence acceleration of Runge-Kutta schemes for solving the Navier–Stokes equations', *Journal of Computational Physics* **224**(1), 365–388.
**URL:** *https://doi.org/10.1016/j.jcp.2007.02.028*

Wang, D. X. and Huang, X. (2017), 'Solution stabilization and convergence acceleration for the harmonic balance equation system', *Journal of Engineering for Gas Turbines and Power* **139**(9), 092503–1.
**URL:** *https://doi.org/10.1115/1.4035912*

Yoon, S. and Jameson, A. (1988), 'Lower-upper symmetric-Gauss-Seidel method for the Euler and Navier-Stokes equations', *AIAA Journal* **26**(9), 1025–1026.
**URL:** *https://doi.org/10.2514/3.10007*

## APPENDIX A - Derivation of Jacobian matrix of spatial discretization operator

Build up the spatial discrete matrix of the convective fluxes $\boldsymbol{C_c}$ with periodic boundary conditions as follow

$$\boldsymbol{C_c} = \begin{pmatrix} (Q_y^{(2)}+Q_x)_1 & (Q_y^{(2)})_1 & & & & (Q_y^{(1)})_{j_m} \\ (Q_y^{(1)})_2 & (Q_y^{(2)}+Q_x)_2 & (Q_y^{(3)})_2 & & & \\ & \ddots & \ddots & \ddots & & \\ & & (Q_y^{(1)})_{j_m-1} & (Q_y^{(2)}+Q_x)_{j_m-1} & (Q_y^{(3)})_{j_m-1} & \\ (Q_y^{(3)})_1 & & & (Q_y^{(1)})_{j_m} & (Q_y^{(2)}+Q_x)_{j_m} & \end{pmatrix} \tag{A1}$$

where the submatrix is given by

$$(Q_y^{(m)})_j = \begin{pmatrix} (q_y^{(m)})_1 & & & \\ & (q_y^{(m)})_2 & & \\ & & \ddots & \\ & & & (q_y^{(m)})_{i_m} \end{pmatrix}_j, m = 1,2,3 \tag{A2}$$

and

$$(Q_x)_j = \begin{pmatrix} (q_x^{(2)})_1 & (q_x^{(3)})_1 & & & (q_x^{(1)})_{i_m} \\ (q_x^{(1)})_2 & (q_x^{(2)})_2 & (q_x^{(3)})_2 & & \\ & \ddots & \ddots & \ddots & \\ & & (q_x^{(1)})_{i_m-1} & (q_x^{(2)})_{i_m-1} & (q_x^{(3)})_{i_m-1} \\ (q_x^{(1)})_1 & & & (q_x^{(1)})_{i_m} & (q_x^{(2)})_{i_m} \end{pmatrix}_j \tag{A3}$$

in which

$$\begin{aligned} (q_x^{(1)})_{i,j} &= -\frac{1}{2}(S_{x,i-\frac{1}{2},j}J_{A,i-1,j} + S_{y,i-\frac{1}{2}}J_{B,i-1},j) \\ (q_x^{(2)})_{i,j} &= \frac{1}{2}[(S_{x,i+\frac{1}{2},j} - S_{x,i-\frac{1}{2}})J_{A,i,j} + (S_{y,i+\frac{1}{2},j} - S_{y,i+\frac{1}{2}},j)J_{B,i,j}] \\ (q_x^{(3)})_{i,j} &= \frac{1}{2}(S_{x,i+\frac{1}{2},j}J_{A,i+1,j} + S_{y,i+\frac{1}{2},j}J_{B,i+1,j}) \end{aligned} \tag{A4}$$

and

$$\begin{aligned} (q_y^{(1)})_{i,j} &= -\frac{1}{2}(S_{x,i,j-\frac{1}{2}}J_{A,i,j-1} + S_{y,i,j-\frac{1}{2}}J_{B,i,j-1}) \\ (q_y^{(2)})_{i,j} &= \frac{1}{2}[(S_{x,i,j+\frac{1}{2}} - S_{x,i,j-\frac{1}{2}})J_{A,i,j} + (S_{y,i,j+\frac{1}{2}} - S_{y,i,j+\frac{1}{2}})J_{B,i,j}] \\ (q_y^{(3)})_{i,j} &= \frac{1}{2}(S_{x,i,j+\frac{1}{2}}J_{A,i,j+1} + S_{n,i,j+\frac{1}{2}}J_{B,i,j+1}) \end{aligned} \tag{A5}$$

It is similar to build up spatial discrete matrix of the dissipative fluxes with periodic boundary conditions

$$\boldsymbol{C_d} = \begin{pmatrix} (D_y^{(3)}+D_x)_1 & (D_y^{(4)})_1 & (D_y^{(5)})_1 & & & (D_y^{(1)})_{j_m-1} & (D_y^{(2)})_{j_m} \\ (D_y^{(2)})_2 & (D_y^{(3)}+D_x)_2 & (D_y^{(4)})_2 & (D_y^{(5)})_2 & & & (D_y^{(1)})_{j_m} \\ \ddots & \ddots & \ddots & \ddots & \ddots & & \\ & (D_y^{(1)})_j & (D_y^{(2)})_j & (D_y^{(3)}+D_x^{(3)})_j & (D_y^{(4)})_j & (D_y^{(5)})_j & \\ & & \ddots & \ddots & \ddots & \ddots & \\ (D_y^{(4)})_1 & & & (D_y^{(1)})_{j_m-1} & (D_y^{(2)})_{j_m-1} & (D_y^{(3)}+D_x)_{j_m-1} & (D_y^{(4)})_{j_m-1} \\ (D_y^{(5)})_2 & (D_y^{(4)})_1 & & & (D_y^{(1)})_{j_m} & (D_y^{(2)})_{j_m} & (D_y^{(3)}+D_x)_{j_m} \end{pmatrix} \tag{A6}$$

where the submatrix is given by

$$(D_y^{(m)})_j = \begin{pmatrix} (d_y^{(m)})_1 & & & \\ & (d_y^{(m)})_2 & & \\ & & \ddots & \\ & & & (d_y^{(m)})_{i_m} \end{pmatrix}_j, m = 1,2,3,4,5 \tag{A7}$$

and

$$(D_x)_j = \begin{pmatrix} (d_x^{(3)})_1 & (d_x^{(4)})_1 & (d_x^{(5)})_1 & & & (d_x^{(1)})_{i_m-1} & (d_x^{(2)})_{i_m} \\ (d_x^{(2)})_2 & (d_x^{(3)})_2 & (d_x^{(4)})_2 & (d_x^{(5)})_2 & & & (d_x^{(1)})_{i_m} \\ \ddots & \ddots & \ddots & \ddots & \ddots & & \\ & (d_x^{(1)})_i & (d_x^{(2)})_i & (d_x^{(3)})_i & (d_x^{(4)})_i & (d_x^{(5)})_i & \\ & & \ddots & \ddots & \ddots & \ddots & \\ (d_x^{(1)})_{i_m-1} & & & (d_x^{(2)})_{i_m-1} & (d_x^{(3)})_{i_m-1} & (d_x^{(4)})_{i_m-1} & (d_x^{(5)})_{i_m-1} \\ (d_x^{(1)})_{i_m} & (d_x^{(2)})_{i_m} & & & (d_x^{(3)})_{i_m} & (d_x^{(4)})_{i_m} & (d_x^{(5)})_{i_m} \end{pmatrix}_j \tag{A8}$$

where

$$\begin{aligned} (d_x^{(1)})_{i,j} &= \Lambda_{i+\frac{1}{2},j}\varepsilon^{(4)}_{i+\frac{1}{2},j} \\ (d_x^{(2)})_{i,j} &= -(3\Lambda_{i+\frac{1}{2},j}\varepsilon^{(4)}_{i+\frac{1}{2},j} + \Lambda_{i-\frac{1}{2},j}\varepsilon^{(4)}_{i-\frac{1}{2}}, j) - \Lambda_{i+\frac{1}{2},j}\varepsilon^{(2)_{i+\frac{1}{2},j}} \\ (d_x^{(3)})_{i,j} &= (3\Lambda_{i+\frac{1}{2},j}\varepsilon^{(4)}_{i+\frac{1}{2},j} + 3\Lambda_{i-\frac{1}{2},j}\varepsilon^{(4)}_{i-\frac{1}{2}}, j) + (\Lambda_{i+\frac{1}{2},j}\varepsilon^{(2)}_{i+\frac{1}{2},j} + \Lambda_{i-\frac{1}{2},j}\varepsilon^{(2)}_{i-\frac{1}{2},j}) \\ (d_x^{(4)})_{i,j} &= -(\Lambda_{i+\frac{1}{2},j}\varepsilon^{(4)}_{i+\frac{1}{2},j} + 3\Lambda_{i-\frac{1}{2},j}\varepsilon^{(4)}_{i-\frac{1}{2}}, j) - \Lambda_{i-\frac{1}{2},j}\varepsilon^{(2)}_{i-\frac{1}{2},j} \\ (d_x^{(5)})_{i,j} &= \Lambda_{i-\frac{1}{2},j}\varepsilon^{(4)}_{i-\frac{1}{2},j} \end{aligned} \tag{A9}$$

and

$$\begin{aligned} (d_y^{(1)})_{i,j} &= \Lambda_{i,j+\frac{1}{2}}\varepsilon^{(4)}_{i,j+\frac{1}{2}} \\ (d_y^{(2)})_{i,j} &= -(3\Lambda_{i,j+\frac{1}{2}}\varepsilon^{(4)}_{i,j+\frac{1}{2}} + \Lambda_{i,j-\frac{1}{2}}\varepsilon^{(4)}_{i,j-\frac{1}{2}}) - \Lambda_{i,j+\frac{1}{2}}\varepsilon^{(2)_{i,j+\frac{1}{2}}} \\ (d_y^{(3)})_{i,j} &= (3\Lambda_{i,j+\frac{1}{2}}\varepsilon^{(4)}_{i,j+\frac{1}{2}} + 3\Lambda_{i,j-\frac{1}{2}}\varepsilon^{(4)}_{i,j-\frac{1}{2}}) + (\Lambda_{i,j+\frac{1}{2}}\varepsilon^{(2)}_{i,j+\frac{1}{2}} + \Lambda_{i,j-\frac{1}{2}}\varepsilon^{(2)}_{i,j-\frac{1}{2}}) \\ (d_y^{(4)})_{i,j} &= -(\Lambda_{i+\frac{1}{2},j}\varepsilon^{(4)}_{i,j+\frac{1}{2}} + 3\Lambda_{i-\frac{1}{2},j}\varepsilon^{(4)}_{i,j-\frac{1}{2}}) - \Lambda_{i,j-\frac{1}{2}}\varepsilon^{(2)}_{i,j-\frac{1}{2}} \\ (d_y^{(5)})_{i,j} &= \Lambda_{i,j-\frac{1}{2}}\varepsilon^{(4)}_{i,j-\frac{1}{2}} \end{aligned} \tag{A10}$$

For different boundary conditions, the submatrix in Eq.(A11) and Eq.(A12) need to be altered as follow

$$\boldsymbol{Cc} = \begin{pmatrix} (Q_y^{(2)} + Q_x)_1 + BC & (Q_y^{(2)})_1 & & & & 0 \\ (Q_y^{(1)})_2 & (Q_y^{(2)} + Q_x)_2 & (Q_y^{(3)})_2 & & & \\ & \ddots & \ddots & \ddots & & \\ & & (Q_y^{(1)})_{j_m-1} & (Q_y^{(2)} + Q_x)_{j_m-1} & (Q_y^{(3)})_{j_m-1} & \\ 0 & & & (Q_y^{(1)})_{j_m} & (Q_y^{(2)} + Q_x)_{j_m} + BC \end{pmatrix} \tag{A11}$$

$$\boldsymbol{C_d} = \begin{pmatrix} (D_y^{(3)} + D_x)_1 + BC & (D_y^{(4)})_1 & (D_y^{(5)})_1 & & & 0 & 0 \\ (D_y^{(2)})_2 + BC & (D_y^{(3)} + D_x)_2 & (D_y^{(4)})_2 & (D_y^{(5)})_2 & & & 0 \\ \ddots & \ddots & \ddots & \ddots & \ddots & & \\ & (D_y^{(1)})_j & (D_y^{(2)})_j & (D_y^{(3)} + D_x^{(3)})_j & (D_y^{(4)})_j & (D_y^{5})_j & \\ & & \ddots & \ddots & \ddots & \ddots & \\ 0 & & & (D_y^{(1)})_{j_m-1} & (D_y^{(2)})_{j_m-1} & (D_y^{(3)} + D_x)_{j_m-1} & (D_y^{(4)})_{j_m-1} + BC \\ 0 & 0 & & & (D_y^{(1)})_{j_m} & (D_y^{(2)})_{j_m} & (D_y^{(3)} + D_x)_{j_m} + BC \end{pmatrix} \tag{A12}$$

where $BC$ is the Jacobian matrix of boundary condition. Then the total spatial discrete matrix $\boldsymbol{C}$ is given by

$$\boldsymbol{C} = \boldsymbol{C_c} + \boldsymbol{C_d} \tag{A13}$$